

that the η of 300 mV for MnO₂ at pH 14 increased significantly to 610 mV at pH 6.5.⁴⁴ Several other manganese oxides, including MnOOH and the mixed oxide of Mn₂O₃ and MnO₂, also require a large η , ranging from 500 to 700 mV, at neutral pH.^{47,49}

For the successful application of Mn catalysts as components for solar fuel production processes, improvement of the water oxidation activity, particularly under neutral conditions, is essential. Nevertheless, few studies have investigated the mechanisms of water oxidation at the surface of manganese oxide electrodes. Thus, the reasons for the sharp decline of the catalytic activity of manganese oxides under neutral conditions remain unclear.

In the present work, we examined the mechanism underlying the pH-dependent activity of water oxidation at the surface of a manganese oxide electrode on the basis of a spectroelectrochemical method. Following the deposition of manganese oxide nanoparticles, δ -MnO₂, onto a fluorine-doped tin oxide (FTO) electrode, we monitored spectral changes during the catalytic cycle of water oxidation at pH ranging from 4 to 13. Using this approach, we succeeded in detecting surface intermediates of O₂ evolution from manganese oxide electrodes that provide new insight into the mechanism for the pH-dependent activity of water oxidation.

2. EXPERIMENTAL SECTION

Manganese oxide electrodes were prepared using a spray deposition method, as previously described.⁵⁴ Briefly, a 0.5 mM MnO₂ colloidal solution was obtained by the reduction of KMnO₄ with a stoichiometric amount of Na₂S₂O₃ at room temperature and was then repeatedly sprayed onto a clean conducting glass substrate (FTO-coated glass, resistance 20 Ω /square, size 30 mm \times 30 mm, SPD Laboratory, Inc.) held on a 200 $^{\circ}$ C hot plate. Each spray application of the solution was followed by a pause of 10 s to allow evaporation of the freshly sprayed solution. This process was repeated 600 times, with a total of approximately 6.0 mL of the MnO₂ solution being deposited on the FTO substrate. The resultant transparent dark-brown film on the electrode was rinsed with pure water and then calcinated at 500 $^{\circ}$ C in air for 2 h. All reagents used were reagent grade and were used without further purification.

Current density (j) vs potential (U) curves were obtained with a commercial potentiostat and potential programmer (HZ-5000, Hokuto Denko) using a Pt wire as the counter electrode and a Ag/AgCl/KCl(satd) electrode as the reference electrode. The electrolyte solution was prepared using highly pure Milli-Q water (18 M Ω ⁻¹ cm⁻¹) and reagent grade chemicals, and the pH was adjusted using 0.1 M H₂SO₄ and 1.0 M NaOH and their mixture. No agent for pH buffering was added to avoid influences from the specific adsorption of multivalent anions.⁵⁵ The prepared electrolyte solution was maintained at 30 $^{\circ}$ C and was bubbled with argon gas prior to the measurements. For minimizing pH changes near the electrode surface, the j vs U curve was measured using a potential sweep from negative to positive without stirring. The amount of dissolved oxygen in the electrolyte was monitored simultaneously with the j vs U measurements using a needle-type oxygen microsensor (Microx TX3-trace, PreSens).

Optical absorption spectra were obtained in diffuse transmission mode using a UV-vis spectrometer (UV-2550, Shimadzu) equipped with a multipurpose large-sample compartment with a built-in integrating sphere (MPC-2200, Shimadzu). For in situ acquisition of spectra, a MnO₂ film electrode mounted in the electrochemical cell was placed in front of the integrating sphere to collect diffused transmission light. The structure of a MnO₂ film was characterized using scanning electron microscopy (SEM; YE-9800 electron microscope, Keyence), high-resolution transmission electron microscopy (HRTEM; H-9000 UHR, 300 kV, Hitachi), and X-ray diffraction (XRD; RINT-2100, Cu $K\alpha$ radiation, Rigaku). For HRTEM analysis, MnO₂ powder was scratched off from the surface of the electrodes,

dispersed into ethanol, and deposited onto germanium-coated microgrids. XRD patterns were recorded from 30 $^{\circ}$ to 70 $^{\circ}$ in 2θ at a step size of 0.02 $^{\circ}$ and a scan rate of 0.25 deg/min. To determine the chemical formula of a MnO₂ electrode, thermal analysis was carried out at a heating rate of 10 $^{\circ}$ C/min to 500 $^{\circ}$ C. The weight loss due to structural water was measured by thermogravimetric analysis (TGA; Thermo plus TG8120, Rigaku). Chemical analysis of the K/Mn ratio was done using atomic absorption spectroscopy (AAS; Z-2000, Hitachi). The average oxidation state of manganese in MnO₂ was determined by the oxalic acid–permanganate back-titration. A 0.1 g sample was dissolved in 10 mL of 0.5 M H₂C₂O₄ and 10 mL of 0.5 M H₂SO₄ to reduce all highly charged manganese ions to Mn²⁺. The excess C₂O₄²⁻ was determined by titration at around 60 $^{\circ}$ C with 0.02 M KMnO₄.

3. RESULTS

3.1. Characterization and Electrocatalytic Potential of MnO₂ Electrodes.

Figure 1a shows the XRD pattern for a

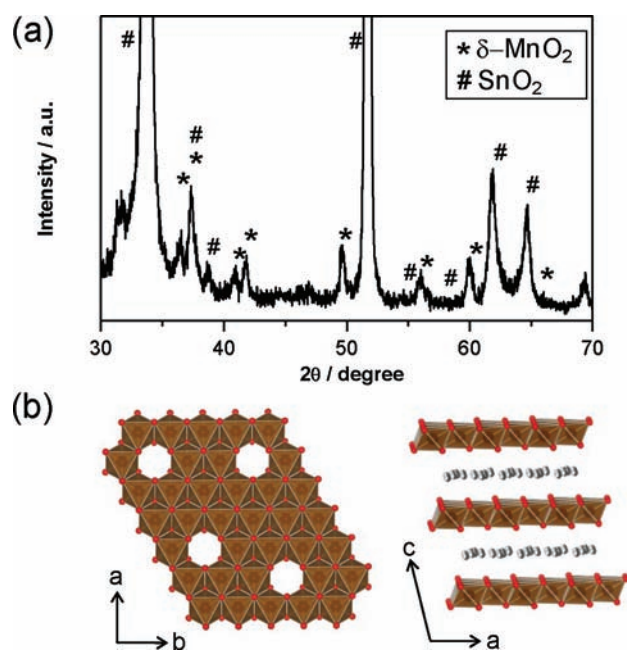


Figure 1. (a) X-ray diffraction pattern of a δ -MnO₂ film on a SnO₂ substrate. The patterns assigned to δ -MnO₂ and SnO₂ are indicated with asterisks and pound signs, respectively. (b) (Left) Schematic arrangement of Mn octahedra in the layer structure of a hexagonal δ -MnO₂. Brown, red, and gray represent Mn, O, and water, respectively. A fraction of the layer Mn⁴⁺ cations are vacant. (Right) Projection of δ -MnO₂ along the b axis. We adopted an image of the crystal structure of δ -MnO₂ intercalated with a water molecule, as the interlayer position was mainly occupied with a water molecule for the prepared δ -MnO₂ (K_{0.17}[Mn⁴⁺_{0.90}Mn³⁺_{0.07}□_{0.03}]O₂·0.53H₂O).

prepared manganese oxide electrode. The electrode exhibited an XRD pattern characteristic of δ -MnO₂ (potassium birnessite, indexed to JCPDS 15-0604), and no peaks assignable to other crystal phases of manganese oxides were detected. As shown in Figure 1b, δ -MnO₂ has a 2-D layered structure composed of edge-sharing MnO₆ octahedra with water molecules and/or metal cations occupying the interlayer region.^{56,57} K⁺ ions served as intercalated cations of the δ -MnO₂ particles. The chemical formula of δ -MnO₂ was expressed with K_{0.17}(Mn⁴⁺_{0.90}Mn³⁺_{0.07}□_{0.03})O₂·0.53H₂O as determined by TGA, AAS, and the oxalic acid–permanganate back-titration. HRTEM analysis combined with electron diffraction measure-

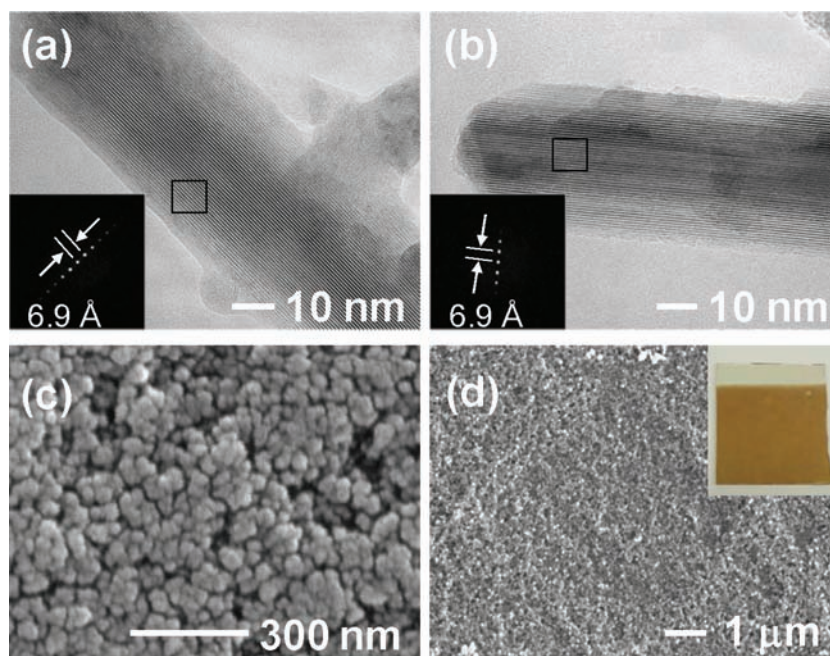


Figure 2. HRTEM images of nanocrystalline δ -MnO₂ (a) before and (b) after electrolysis in a 0.5 M Na₂SO₄ aqueous solution at 1.9 V for 30 min. The insets show FFT analysis results for the outlined areas in the crystal. (c, d) SEM images and a photograph (inset) of the as-prepared δ -MnO₂ film.

ments showed that the δ -MnO₂ particles in the electrode film adopted a 2-D layered structure with an interlayer distance of 6.9 Å, which is characteristic for a (110) plane of K⁺ ion intercalated δ -MnO₂ (Figure 2a).^{58,59} SEM observations demonstrated that the entire electrode surface of the FTO substrate was covered with nanoparticles with diameters ranging from 20 to 50 nm (Figure 2c,d).

A representative j - U curve for the δ -MnO₂ electrode measured at neutral pH (0.5 M Na₂SO₄, pH 6) is shown in Figure 3. An increase in both anodic current (solid line) and O₂

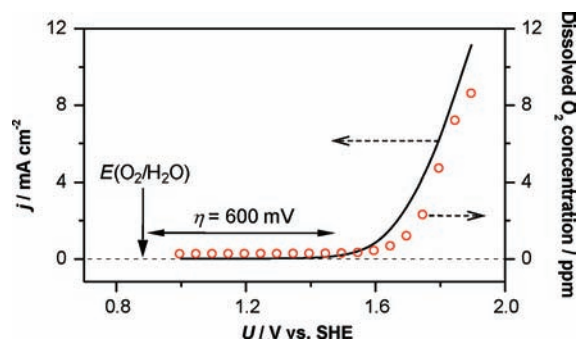


Figure 3. Current density (solid line) and dissolved O₂ concentration (open circles) for a δ -MnO₂ film electrode in a 0.5 M Na₂SO₄ aqueous solution (pH 6) during the positive potential sweep at 10 mV/s. $E(\text{O}_2/\text{H}_2\text{O})$ reflects the standard potential for O₂ evolution.

production (open circles) was observed at an onset potential of approximately 1.5 V. Since O₂ production by a bare FTO electrode was not detected (Figure S1, Supporting Information), the observed water oxidation current generated by the δ -MnO₂ electrode was attributable to the electrocatalytic function of the δ -MnO₂ nanoparticles. The δ -MnO₂ electrode was next subjected to HRTEM analysis after electrolysis for 30 min at 1.9 V, corresponding to a turnover number of 72 (evolved O₂

molecules per Mn atom) (Figure 2). The HRTEM images in Figure 2b show that the δ -MnO₂ nanoparticles maintained an interlayer distance of 6.9 Å, confirming the stability of δ -MnO₂ for water oxidation. However, the δ -MnO₂ electrode exhibited a remarkably large deviation of 600 mV in the onset of anodic current, $U_{\text{on},j}$, from the standard potential for O₂ evolution (Figure 3). The η of 600 mV is a typical value reported for manganese oxide electrocatalysts at neutral pH.^{44,47,49,50,53,60} We next examined the origin for the large η using UV-vis spectroelectrochemical methods.

3.2. In Situ Spectroscopic Analysis of Surface Intermediates. **3.2.1. Spectral Changes Associated with Water Oxidation at Neutral pH.** The δ -MnO₂ electrode displayed an intense absorption in the UV and visible light region that was assigned to its band gap transition (Figure 4a, trace 1).^{61,62} This characteristic allowed us to apply an in situ spectroelectrochemical method to elucidate the origin of η and the mechanisms underlying its pH dependence.

First, we examined the spectral changes of the δ -MnO₂ electrode caused by water oxidation at neutral pH (0.5 M Na₂SO₄, pH 6) (Figure 4b). Diffuse transmission UV-vis absorption spectra were recorded in 0.5 M Na₂SO₄ at potentials ranging from 1.2 to 1.8 V using the spectral data obtained at 1.1 V as a spectral reference. Upon stepping U from 1.2 to 1.8 V in 0.1 V increments, a new absorption peak at 510 nm, ΔAbs_{510} , and bleaching of the absorption in the longer wavelength region of the band gap transition, $\Delta\text{Abs}_{>680}$, were observed, in addition to a clear isosbestic point at 680 nm (Figure 4b). These spectral changes were fully reversible for both the positive- and negative-going sweeps and remained stable in the repeated cycle of the potential sweep (Figure S2, Supporting Information).

As seen from the plot of ΔAbs_{510} (filled circles) against U in Figure 5, ΔAbs_{510} was negligible in the potential range of 1.1–1.3 V, but increased rapidly at more positive potentials. The depression of $\Delta\text{Abs}_{>680}$ exhibited a potential-dependent

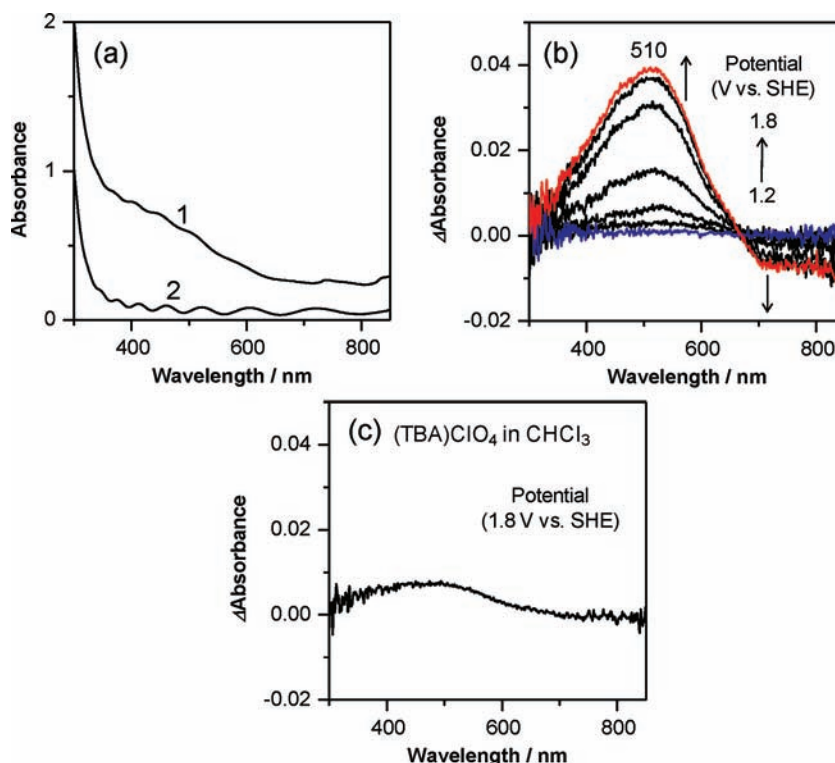


Figure 4. (a) Diffuse transmission UV-vis absorption spectra of (1) a δ -MnO₂ film electrode and (2) a bare FTO electrode. (b) Changes in the UV-vis spectrum of a δ -MnO₂ film electrode at increasing potential (1.2, 1.3, 1.4, 1.5, 1.6, 1.7, and 1.8 V). The spectrum measured at 1.1 V was used as a reference spectrum. Arrows indicate the direction of a spectral change with a potential shift from 1.2 to 1.8 V. The spectra at 1.2 and 1.8 V were colored blue and red, respectively. (c) Difference spectrum of a δ -MnO₂ film electrode at 1.8 V in a 0.1 M (TBA)ClO₄ in CHCl₃ solution. The spectrum measured at 1.1 V was used as a reference spectrum.

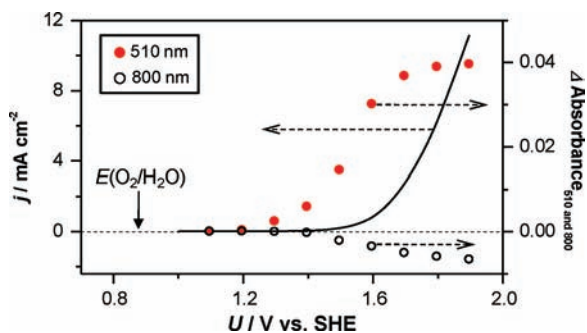


Figure 5. Potential dependences of the difference absorbance at 510 nm (filled circles) and 800 nm (open circles) for a δ -MnO₂ electrode in a 0.5 M Na₂SO₄ aqueous solution (pH 6). The solid line indicates a j - U curve for a δ -MnO₂ electrode obtained in a 0.5 M Na₂SO₄ aqueous solution.

behavior resembling that of j - U and ΔAbs_{510} - U relations (open circles). Note that when an organic electrolyte, a chloroform solution containing tetra-*n*-butylammonium perchlorate ((TBA)ClO₄ in CHCl₃), was used in place of the aqueous solution of 0.5 M Na₂SO₄, both the appearance of ΔAbs_{510} and depression of $\Delta\text{Abs}_{>680}$ were largely suppressed (Figure 4c). Therefore, it is considered that the spectral changes observed in Figures 4 and 5 were the consequence of manganese redox chemistry in the presence of water. In addition, the isosbestic change detected in the spectra indicated that the Mn species responsible for $\Delta\text{Abs}_{>680}$ (species A_{>680}) were transformed into those responsible for ΔAbs_{510} (species A₅₁₀) with the progress of water oxidation.

3.2.2. Effects of pH on Spectral Changes. We next examined the influences of pH on the observed spectral changes of the δ -MnO₂ electrode in conjunction with the pH dependence of η . Figure 6 shows the plot of ΔAbs_{510} against U , together with the j - U curve for δ -MnO₂ electrodes measured at pH ranging from 4 to 13.⁶³ At all examined pH values, the anodic current was assignable to the O₂ evolution reaction (Figure S3, Supporting Information). Figure 7 summarizes the pH dependence of $U_{\text{on},j}$ and $U_{\text{on},A_{510}}$ from the results presented in Figure 6 and also includes the $E(\text{O}_2/\text{H}_2\text{O})$ value to compare η at different pH values. The electrode potential at which the current density for O₂ evolution reached 40 $\mu\text{A cm}^{-2}$ was adopted as $U_{\text{on},j}$. As shown in Figure 7, $U_{\text{on},j}$ (red squares) remained constant at approximately 1.5 V between pH 4 and pH 8, but displayed a sharp negative shift at pH ≥ 9 , which is responsible for the unique pH dependence of η . Namely, η increased from 500 to 700 mV between pH 4 and pH 8, but sharply decreased to 480 mV at pH 9. Moreover, η decreased to 380 mV at pH ≥ 11 . Note that such a non-Nernstian behavior of $U_{\text{on},j}$ was reasonably well reproduced by the pH dependence of $U_{\text{on},A_{510}}$ (Figure 7, blue circles). In addition, it is notable that $U_{\text{on},A_{510}}$ was located at the potential region slightly negative of $U_{\text{on},j}$ over the entire evaluated pH range (Figure 7). These observations indicate that species giving the 510 nm absorption (species A₅₁₀) may serve as precursors for O₂ evolution, and the easiness of species A₅₁₀ production determines the deviation of $U_{\text{on},j}$ from $E(\text{O}_2/\text{H}_2\text{O})$. We could not assign the 510 nm absorption on the basis of the existing spectroscopic data of manganese oxides. Thus, we next attempted to experimentally

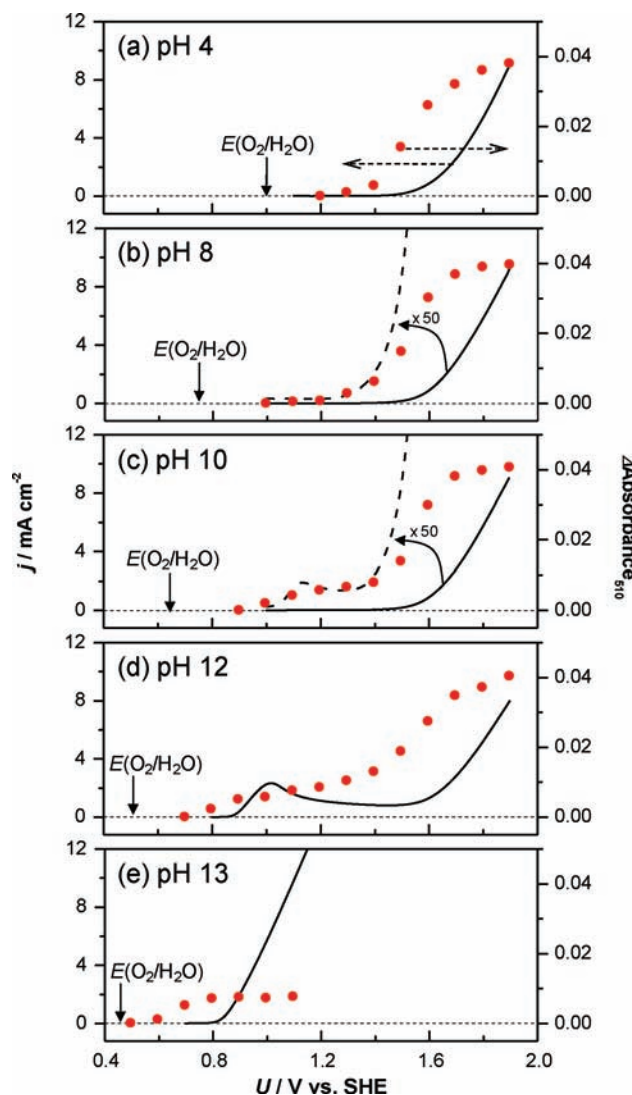


Figure 6. Potential dependences of the current density (solid line) and difference absorbance at 510 nm (filled circles) observed in a 0.5 M Na₂SO₄ aqueous solution at (a) pH 4, (b) pH 8, (c) pH 10, (d) pH 12, and (e) pH 13. The dotted line in (b) and (c) indicates the voltammogram expanded in the y axis direction by a factor of 50. When j - U curves were measured at pH 10 and 12 with stirring electrolyte solutions, an anodic current displayed a continuous increase with potential similar to the case observed at pH 13. (Figure S5, Supporting Information). Therefore, a slight decrease in current density at the potential region between the potential for the first rise of current and 1.5 V observed at pH 10 and 12 is due to the proton accumulation caused by water oxidation (c, d).

determine the chemical origin of the precursors for O₂ evolution.

3.2.3. Redox Potential of Species A₅₁₀. To determine the chemical origin of species A₅₁₀, we first estimated the redox potential of surface intermediates formed on δ -MnO₂ electrodes using the method developed by Wilson⁶⁴ and Salvador et al.⁶⁵ This method is based on the detection of a transient cathodic current when the potential is swept toward the negative following O₂ evolution by a metal oxide electrode at an anodic potential, which is attributable to the surface intermediates formed during water oxidation.^{64,65} Here, using a δ -MnO₂ electrode that had been subjected to water oxidation at 1.8 V for 15 s in 0.5 M Na₂SO₄, the potential was swept

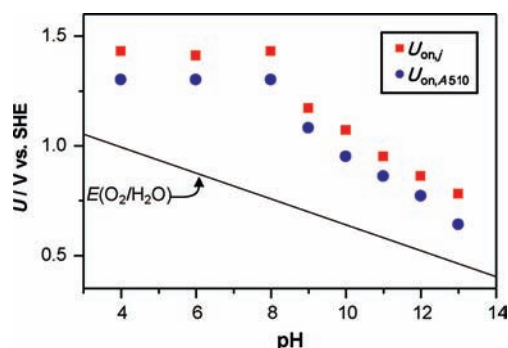


Figure 7. pH dependences of the onset potential for oxidation current ($U_{\text{on},j}$, red squares) and optical absorption at 510 nm ($U_{\text{on},A_{510}}$, blue circles). The solid line represents the standard potential for oxygen evolution.

toward the negative at a scan rate of 50 mV s⁻¹. The change in the absorption peak at 510 nm was also monitored simultaneously with the j - U curve measurements.

In the cathodic potential sweep, a cathodic current started to flow at 1.45 V, with the maximum current detected at 1.35 V (Figure 8a, solid line). Notably, a cathodic current was absent

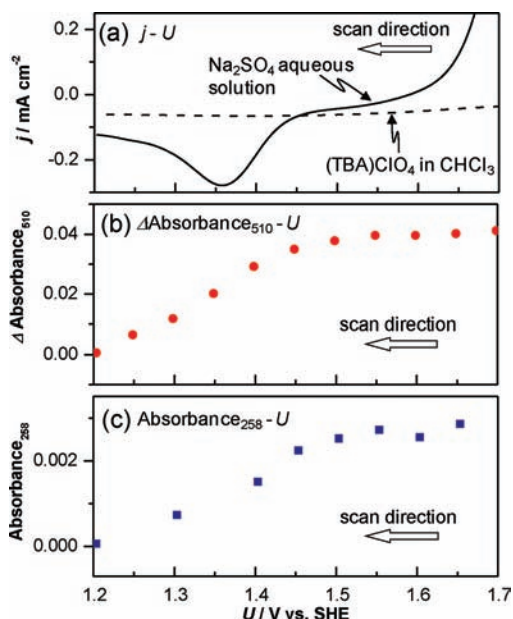


Figure 8. (a) Negative linear sweep voltammograms obtained in a 0.5 M Na₂SO₄ solution (pH 6) (solid line) and a 0.1 M (TBA)ClO₄ in CHCl₃ solution (dotted line) after electrolysis at 1.8 V for 15 s. The scan rate was 50 mV s⁻¹. (b) Potential dependence of the difference absorbance at 510 nm during the negative-going linear sweep voltammetry measurement from 1.8 to 1.2 V in a 0.5 M Na₂SO₄ solution at pH 6. The absorbance obtained at 1.2 V was used as a reference. (c) Potential dependence of absorbance at 258 nm during the negative-going linear sweep voltammetry measurement from 1.8 to 1.2 V in a 0.5 M Na₂SO₄ solution at pH 6. The absorbance at 258 nm is assigned to the Mn³⁺-pyrophosphate (PP) complex generated by the reaction of surface Mn³⁺ species with 20 mM PP at different electrode potentials.

for the δ -MnO₂ electrode that had been subjected to polarization at 1.8 V in a (TBA)ClO₄ in CHCl₃ solution prior to the potential sweep (Figure 8a, dotted line). On the basis of these results, we can assume that the transient cathodic

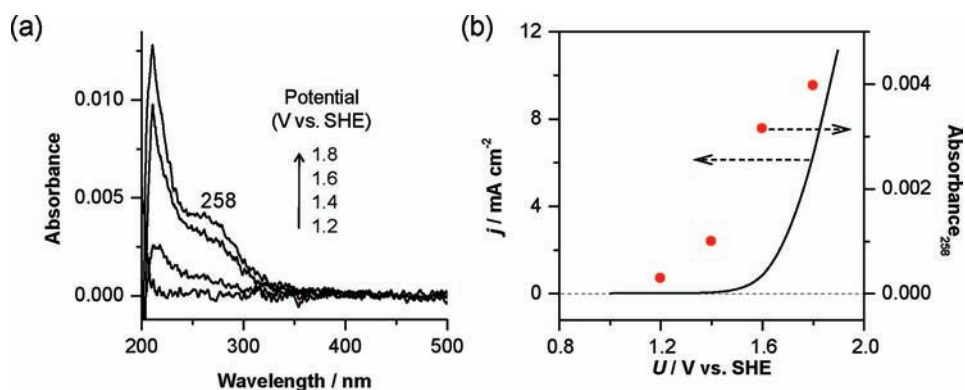


Figure 9. (a) UV-vis absorption spectra of a 20 mM pyrophosphate solution exposed to a δ -MnO₂ electrode after electrolysis in a 0.5 M Na₂SO₄ solution (pH 6). A 20 mM pyrophosphate solution was used as a spectral reference. Electrolysis was conducted for 15 min at electrode potentials of 1.2, 1.4, 1.6, and 1.8 V. The arrow indicates the direction of the spectral change with a potential shift from 1.2 to 1.8 V. (b) Absorbance at 258 nm for a 20 mM pyrophosphate solution as a function of the electrode potential. The solid line shows a j - U curve obtained at pH 6.

current was due to the electroreduction of the surface intermediates related to water oxidation by the δ -MnO₂ electrode. Importantly, transient absorption at 510 nm was also observed during the flow of transient cathodic current (Figure 8b). The agreement between the potential dependence of the transient current and the absorption at 510 nm confirmed that the surface intermediate that generated the transient cathodic current was assignable to species A₅₁₀.

The number of electrons (n) required for the production of species A₅₁₀ was estimated from the half-width potential of the transient cathodic peak, $\Delta E_{p/2}$, using the relation $\Delta E_{p/2} = 3.53RT/nF$ ($= 92.2/n$ at 30 °C).⁶⁶ The $\Delta E_{p/2}$ value was determined to be 100 mV, corresponding to an n of 1. Therefore, we concluded that species A₅₁₀ have a one-electron redox potential located at approximately 1.4 V, although the precise determination of the redox potential was not possible due to the lack of a counterpart anodic wave. Of the reported multiple redox couples involving a Mn center in hydroxides or aquo complexes, only a Mn³⁺/Mn²⁺ couple (Mn³⁺ + e⁻ → Mn²⁺, $E = 1.5$ V^{67,68}) has a one-electron redox potential close to that estimated for species A₅₁₀. Thus, we speculate that Mn³⁺ species existing on the surface of a δ -MnO₂ electrode is a plausible candidate of species A₅₁₀. Here, the amount of species A₅₁₀ was estimated to be 14 nmol from the coulombs of the transient cathodic peak (Figure 8a, solid line), which corresponds to approximately 1% of the total Mn atoms deposited on the electrode.

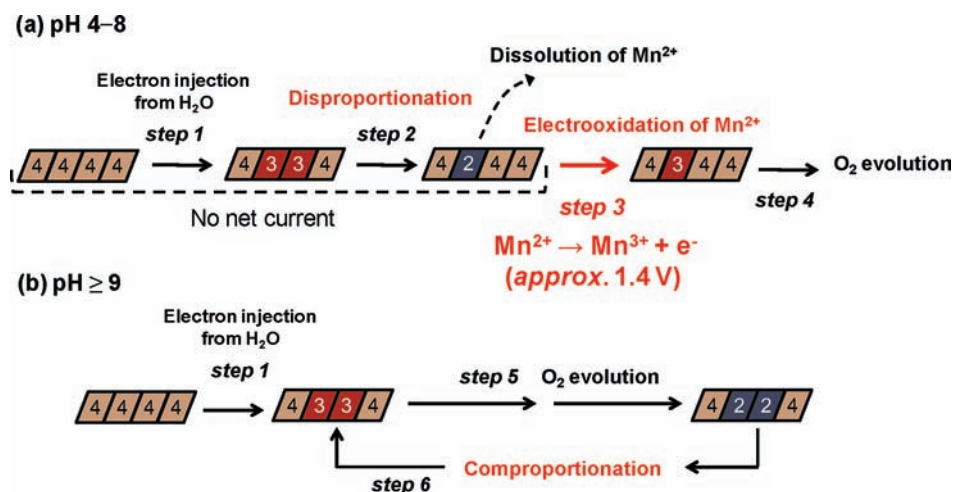
3.2.4. Direct Detection of Mn³⁺ with Pyrophosphate. To obtain solid evidence for the assumption that species A₅₁₀ is attributable to Mn³⁺, we employed pyrophosphate (PP), P₂O₇⁴⁻, as a probe agent for the detection of Mn³⁺. PP is a redox-inert molecule that can uptake Mn³⁺ from the surface of solid-phase manganese oxides via a specific chelating reaction.^{69,70} To assay for Mn³⁺, a δ -MnO₂ electrode was first exposed to a 20 mM PP solution for 15 min to remove the Mn³⁺ ions which were originally contained in the δ -MnO₂ electrodes. The electrode was then subjected to water oxidation in 0.5 M Na₂SO₄. After electrolysis for 15 min, the electrochemical cell was switched to an open circuit condition and the δ -MnO₂ electrode was exposed immediately to a fresh electrolyte solution containing 20 mM PP. The detection of Mn³⁺-PP complexes in solution was then performed by optical absorption measurements (Figure 9).⁷¹ This assay was performed at potentials ranging from 1.2 to 1.8 V to examine

the potential dependence of Mn³⁺ generation. From the UV-vis absorption spectra shown in Figure 9a, clear evidence for the production of Mn³⁺ on the δ -MnO₂ electrode surface can be seen. Namely, the 258 nm absorption peak assigned to a Mn³⁺-PP complex (Figure S4, Supporting Information)⁷¹ was resolved in the potential range of 1.4–1.8 V (Figure 9a). Note that the growth of the 258 nm peak became prominent with increasing U (Figure 9b, filled circles), displaying essentially the same potential dependence as j and ΔAbs_{510} . As a control experiment, when a PP solution reacted with the electrolyte which was taken from the electrochemical reactor after water oxidation at 1.8 V for 15 min, no Mn³⁺-PP was detected, confirming that the observed Mn³⁺-PP was predominantly generated by the reaction of PP with Mn³⁺ adsorbed on the electrode surface. Thus, the probing experiments with PP provide strong support for the assignment of species A₅₁₀ as surface-associated Mn³⁺.

We also conducted the probing experiments with PP to estimate the redox potential of Mn³⁺ adsorbed on the electrode surface using the same voltammetry technique described in Figure 8. Namely, the potential of a δ -MnO₂ electrode that had been subjected to water oxidation at 1.8 V for 15 s in 0.5 M Na₂SO₄ was swept toward the negative from 1.8 to 1.2 V. As shown in Figure 8c, the 258 nm absorption peak assigned to a Mn³⁺-PP complex showed a depression in intensity at a potential of approximately 1.4 V. Of particular note is that the observed depression of the 258 nm absorption peak exhibited essentially the same potential dependence as ΔAbs_{510} - U relations (see Figure 8b). This agreement between the potential-dependent formation of a Mn³⁺-PP complex and species A₅₁₀ further supports the aforementioned assignment and indicates that the one-electron redox potential of Mn³⁺ adsorbed on the surface of the δ -MnO₂ electrode is approximately 1.4 V. The amount of Mn³⁺ remaining on the electrode surface that had been subjected to water oxidation at 1.8 V for 15 min was estimated to be 2.4 nmol from the absorbance at 258 nm (Mn³⁺-PP, $\epsilon = 6750$ M⁻¹ cm⁻¹) (Figure 9a; Figure S4, Supporting Information). This was approximately one-sixth of that estimated from the coulombs of the transient cathodic peak (Figure 8a).

4. DISCUSSION

Now, let us consider the origin and mechanisms underlying the pH dependence of η for water oxidation by a δ -MnO₂

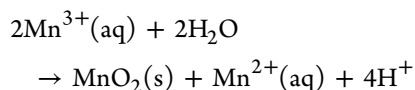
Scheme 1. Oxidation States of Mn Ions Involved in the Electrooxidation of Water to Oxygen on a δ -MnO₂ Electrode at (a) pH 4–8 and (b) pH ≥ 9 ^a

^aLayer Mn atoms are shown as squares. The numbers on the face of the square refer to the sequence of Mn valency. As long as the electrooxidation of Mn²⁺ to Mn³⁺ is the rate-determining step for the O₂ evolution (pH 4–8), further oxidation of H₂O to peroxy species, peroxy species to O₂, or Mn³⁺ to Mn⁴⁺ (or higher valence states such as Mn⁵⁺, Mn⁶⁺, and Mn⁷⁺) will not influence U_{onj} . The amount of Mn³⁺ generated under the catalytic cycle of water oxidation at 1.8 V (pH 6) was 14 nmol at the lowest estimate, which is 1% of the total Mn atoms deposited on the FTO electrode.

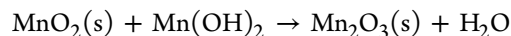
electrode. As summarized in Figure 7, U_{onj} showed non-Nernstian behavior, resulting in unique variations of η with changes in pH. Specifically, η increased from 500 to 700 mV with a rise of pH from 4 to 8, but sharply decreased to 480 mV at pH ≥ 9 . This finding indicates that fundamentally different mechanisms exist for water oxidation under neutral and basic conditions. Although several studies have also demonstrated that strongly alkaline solutions are advantageous for water oxidation by manganese oxide electrodes in terms of η ,^{44–53,60} prior to the present study, the mechanism responsible for this phenomenon had not been determined.

The pH dependence of η might be due to changes in the surface charge of manganese oxide electrodes caused by pH-dependent protonation/deprotonation of surface oxygen species. At low pH, manganese oxide surfaces are protonated and thus have a positive charge.⁷² With increasing pH, however, deprotonation of the surface occurs, resulting in a negative charge.⁷² As the nucleophilicity of oxygen species such as O⁻ in Mn⁴⁺O⁻ is stronger than that of positively charged species, a lower η for water oxidation is expected in basic solutions than those at acidic/neutral pH.⁷³ However, the pK_2 of δ -MnO₂ is reported to be 2.4,⁷⁴ a value in discordance with our present results that show η sharply decreased at pH 9 (Figure 7). Thus, the protonation/deprotonation of oxygen species is likely not the primary reason for the pH dependence of η .

The present observation that species A₅₁₀ which is attributable to surface-associated Mn³⁺ acts as a precursor for O₂ evolution provides an alternative mechanism for the pH dependence of η . The trivalent state of Mn is implicated in disproportionation and comproportionation reactions, whose efficiency sharply varies with pH.^{67,75–77} For example, in acidic/neutral solutions, Mn³⁺ ions are unstable relative to the disproportionation into Mn²⁺ and Mn⁴⁺, as shown in the following reaction:



With increasing pH, however, Mn³⁺ ions are free from the disproportionation reaction and are effectively stabilized by a comproportionation reaction at high pH:



If we adopt the equilibrium constants reported for the disproportionation and comproportionation reactions of β -MnO₂ ($K_{\text{disp}} = 7.87 \times 10^8$ and $K_{\text{comp}} = 1.27 \times 10^{-9}$),⁶⁸ the concentration of Mn³⁺ is estimated to be less than 10⁻¹⁴% of the initial concentrations of MnO₂(s) and Mn²⁺(aq) at pH 6. Meanwhile, in basic solutions, the Mn³⁺ is stabilized by comproportionation and reaches a concentration as high as 99.9%. These estimations indicate that the production and accumulation efficiencies of Mn³⁺ (species A₅₁₀) on the surface of MnO₂ electrodes are remarkably higher at alkaline compared to neutral pH. In other words, at intermediate pH, Mn³⁺ is highly unstable and unable to exist on the surface of MnO₂ electrodes. Therefore, the effective production and accumulation of species A₅₁₀ are expected to occur when the electrode is anodically poised at more positive U than $E(\text{Mn}^{3+}/\text{Mn}^{2+})$.

Silvester et al. have examined the pH dependence of Mn³⁺ disproportionation in δ -MnO₂ particles using extended X-ray absorption fine structure (EXAFS) and XRD measurements.^{78,79} Their detailed analysis showed that the Mn³⁺ in the MnO₂ layer rapidly disproportionates into Mn⁴⁺ and Mn²⁺ in the pH region of 2–5, with the resultant Mn²⁺ being dissolved in the solution phase. In addition, they showed that the disproportionation of Mn³⁺ was fully suppressed at pH ≥ 9 ,^{78,79} which enables the Mn³⁺ to remain in the MnO₂ layers of δ -MnO₂. Here, good agreement was observed between the pH regions where the disproportionation of Mn³⁺ in the MnO₂ layers was suppressed and U_{onj} sharply shifted from 1.5 to 1.2 V (Figures 6 and 7). Moreover, ΔAbs_{510} , which is assigned to the surface Mn³⁺ species acting as precursors of water oxidation, also showed a sharp negative shift of onset potential, $U_{on,A510}$, at the same pH region (Figures 6 and 7). Therefore, we can consider that the pH-dependent disproportionation shown

in Scheme 1 represents one of the most plausible mechanisms for the observed sharp variations of η with changes of pH.

On the basis of the experiments performed in a (TBA)ClO₄ in CHCl₃ solution (Figures 4c and 8a), the formation of Mn³⁺ should proceed via the electron injection from H₂O to anodically poised δ -MnO₂ (step 1, Scheme 1). It is notable that the Mn³⁺ in δ -MnO₂ takes a high spin state ($t_{2g}^3e_g$), and thus, a band gap energy of δ -MnO₂ corresponds to the energy difference between the t_{2g} and e_g states of the Mn 3d orbital.⁸⁰ Thus, the observed bleaching of $\Delta\text{Abs}_{>680}$ that accompanied the growth of ΔAbs_{510} (Figures 4b and 5) can be reasonably attributable to the increased band-gap energy of δ -MnO₂ via the reduction of Mn⁴⁺ to Mn³⁺.⁸⁰ Step 1 may become progressive with increasing U ; however, at pH < 9, Mn³⁺ is rapidly consumed by disproportionation to form Mn²⁺ and Mn⁴⁺, resulting in no net charges passing across the electrode (step 2). Therefore, the effective production of Mn³⁺ requires the electrochemical oxidation of Mn²⁺ to Mn³⁺ (step 3). As long as step 3 is the rate-determining step for the overall water oxidation reaction, further oxidation of H₂O to peroxy species, peroxy species to O₂, or Mn³⁺ to Mn⁴⁺ (or higher valence states such as Mn⁵⁺, Mn⁶⁺, and Mn⁷⁺) will not influence $U_{\text{on},j}$.⁸¹ The fixed $U_{\text{on},j}$ and $U_{\text{on},A_{510}}$ at approximately 1.5 V between pH 4 and pH 9 (Figures 6 and 7) are consistent with our assignment of Mn³⁺ as a precursor for O₂ evolution and demonstrate that step 3 determines the extent of η at pH < 9.

In contrast to the intermediate pH conditions, Mn³⁺ disproportionation is effectively suppressed at pH \geq 9, as reported by Silvester et al.,^{78,79} which results in the accumulation of Mn³⁺ in the MnO₂ layers being very facile. Moreover, in this pH region, the comproportionation reaction between Mn²⁺ and Mn⁴⁺ contributes to the regeneration process of Mn³⁺ (step 6). As abundant Mn⁴⁺ neighbors exist for Mn²⁺ in the MnO₂ layers, the regeneration of Mn³⁺ via step 6 becomes prominent in conjunction with the production of Mn²⁺. Notably, if we assume that Mn³⁺ also acts as a precursor (i.e., an oxidant) for O₂ evolution, similarly to the case at pH < 9, Mn³⁺ production clearly becomes autocatalytic,⁸² as reported for H₂O₂ oxidation by MnO₂ in alkaline conditions.⁷⁶ Under these conditions, Mn³⁺ should be regenerated even in potential regions that are more negative than $E(\text{Mn}^{3+}/\text{Mn}^{2+})$. This speculation is supported by the large negative shift of both $U_{\text{on},j}$ and $U_{\text{on},A_{510}}$ detected at pH \geq 9 and helps explain why η for water oxidation markedly decreased in strongly alkaline solution (Figures 6 and 7).

CONCLUSIONS

In this study, we have revealed the optical absorption spectrum of the precursor for electrooxidation of H₂O to O₂ on δ -MnO₂ electrodes. Detailed investigations of the pH dependence of $j-U$ and $\Delta\text{Abs}_{510}-U$, together with probing experiments for Mn³⁺ using P₂O₇⁴⁻, demonstrated that the Mn³⁺ adsorbed on the electrodes is the precursor for the electrooxidation reaction. On the basis of this finding, we conclude that the large η at pH < 9 is due to the rapid consumption of Mn³⁺ by the disproportionation reaction. Our findings also suggest that the comproportionation between Mn²⁺ and Mn⁴⁺ to form Mn³⁺ occurs at pH \geq 9, which results in a large decrease in η . To our knowledge, this represents the first in situ spectroscopic detection of intermediates for the O₂ evolution reaction mediated by manganese oxides. Thus, the influence of pH on the production efficiency and accumulation of Mn³⁺ demon-

strated here would be important for development of manganese oxide electrocatalysts that can serve as efficient water oxidation catalysts at intermediate pH.

ASSOCIATED CONTENT

Supporting Information

Additional plots of difference absorbance, dissolved oxygen as a function of the electrode potential, and negative-going linear sweep voltammograms. This material is available free of charge via the Internet at <http://pubs.acs.org>.

AUTHOR INFORMATION

Corresponding Author

hashimoto@light.t.u-tokyo.ac.jp; nakamura@light.t.u-tokyo.ac.jp

ACKNOWLEDGMENTS

This work was financially supported by the Exploratory Research for Advanced Technology (ERATO) program of the Japan Science and Technology Agency (JST) and partially by a Grant-in-Aid for Scientific Research on Priority Areas from the Ministry of Education, Culture, Sports, Science, Technology (MEXT) of the Japanese Government (21750186), The Canon Foundation, and Research Fellowships of the Japan Society for Promotion of Science (JSPS) for Young Scientists (Grant 21-9161).

REFERENCES

- (1) Fujishima, A.; Honda, K. *Nature* **1972**, *238*, 37.
- (2) Nozik, A. J. *Annu. Rev. Phys. Chem.* **1978**, *29*, 189.
- (3) Bard, A. J.; Fox, M. A. *Acc. Chem. Res.* **1995**, *28*, 141.
- (4) Lewis, N. S.; Nocera, D. G. *Proc. Natl. Acad. Sci. U.S.A.* **2006**, *103*, 15729.
- (5) Zhao, Y.; Hernandez-Pagan, E. A.; Vargas-Barbosa, N. M.; Dysart, J. L.; Mallouk, T. E. *J. Phys. Chem. Lett.* **2011**, *2*, 402.
- (6) Morris, N. D.; Suzuki, M.; Mallouk, T. E. *J. Phys. Chem. A* **2004**, *108*, 9115.
- (7) Lodi, G.; Sivieri, E.; De Battisti, A.; Trasatti, S. *J. Appl. Electrochem.* **1978**, *8*, 135.
- (8) Nakagawa, T.; Beasley, C. A.; Murray, R. W. *J. Phys. Chem. C* **2009**, *113*, 12958.
- (9) Yagi, M.; Tomita, E.; Sakita, S.; Kuwabara, T.; Nagai, K. *J. Phys. Chem. B* **2005**, *109*, 21489.
- (10) Mills, A.; Russell, T. *J. Chem. Soc., Faraday Trans.* **1991**, *87*, 1245.
- (11) Harriman, A.; Pickering, I. J.; Thomas, J. M.; Christensen, P. A. *J. Chem. Soc., Faraday Trans. 1* **1988**, *84*, 2795.
- (12) Han, H.; Frei, H. *J. Phys. Chem. C* **2008**, *112*, 16156.
- (13) Nakamura, R.; Frei, H. *J. Am. Chem. Soc.* **2006**, *128*, 10668.
- (14) Howells, A. R.; Sankarraj, A.; Shannon, C. *J. Am. Chem. Soc.* **2004**, *126*, 12258.
- (15) Satorel, A.; Carraro, M.; Scorrano, G.; Zorzi, R. D.; Geremia, S.; McDaniel, N. D.; Bernhard, S.; Bonchio, M. *J. Am. Chem. Soc.* **2008**, *130*, 5006.
- (16) Geletii, Y. V.; Huang, Z.; Hou, Y.; Musaev, D. G.; Lian, T.; Hill, C. L. *J. Am. Chem. Soc.* **2009**, *131*, 7522.
- (17) Kanan, M. W.; Nocera, D. G. *Science* **2008**, *321*, 1072.
- (18) Kay, A.; Cesar, I.; Gratzel, M. *J. Am. Chem. Soc.* **2006**, *128*, 15714.
- (19) Sivula, K.; Zboril, R.; Formal, F. L.; Robert, R.; Weidenkaft, A.; Tucek, J.; Frydrych, J.; Gratzel, M. *J. Am. Chem. Soc.* **2010**, *132*, 7436.
- (20) Jiao, F.; Frei, H. *Angew. Chem., Int. Ed.* **2009**, *48*, 1841.
- (21) Esswein, A. J.; McMurdo, M. J.; Ross, P. N.; Bell, A. T.; Tilley, T. D. *J. Phys. Chem. C* **2009**, *113*, 15068.

- (22) Ahmad, J.; Kumar, B.; Mugweru, A. M.; Trinh, P.; Ramanujachary, K. V.; Lofland, S. E.; Govind.; Ganguli, A. K. *J. Phys. Chem. C* **2010**, *114*, 18779.
- (23) Zhong, D. K.; Sun, J.; Inumura, H.; Gamelin, D. R. *J. Am. Chem. Soc.* **2009**, *131*, 6086.
- (24) Silva, C. G.; Boizi, Y.; Fornes, V.; Garcia, H. *J. Am. Chem. Soc.* **2009**, *131*, 13833.
- (25) Yin, Q.; Tan, J. M.; Besson, C.; Geletii, Y. V.; Musaev, D. G.; Kuznetsov, A. E.; Luo, Z.; Hardcastle, K. I.; Hill, C. L. *Science* **2010**, *328*, 342.
- (26) Siegbahn, P. E. M. *Acc. Chem. Res.* **2009**, *42*, 1871.
- (27) Armstrong, F. A. *Philos. Trans. R. Soc. London, Ser. B* **2008**, *363*, 1263.
- (28) Tributsch, H. *Electrochim. Acta* **1994**, *39*, 1495.
- (29) Tributsch, H. *J. Electroanal. Chem.* **1992**, *331*, 783.
- (30) Vass, I.; Styring, S. *Biochemistry* **1991**, *30*, 830.
- (31) Geijer, P.; Morvaridi, F.; Styring, S. *Biochemistry* **2001**, *40*, 10881.
- (32) Metz, J. G.; Nixon, P. J.; Rogner, M.; Brudvig, G. W.; Diner, B. A. *Biochemistry* **1989**, *28*, 6960.
- (33) Umena, Y.; Kawakami, K.; Shen, J.; Kamiya, N. *Nature* **2011**, *472*, 55.
- (34) Yano, J.; Kern, J.; Sauer, K.; Latimer, M. J.; Puskar, Y.; Biesiadka, J.; Loll, B.; Saenger, W.; Messinger, J.; Zouni, A.; Yachandra, V. K. *Science* **2006**, *314*, 821.
- (35) Robinson, D. M.; Go, Y. B.; Greenblatt, M.; Dismukes, G. C. *J. Am. Chem. Soc.* **2010**, *132*, 11467.
- (36) Najafpour, M. M.; Ehrenberg, Till.; Wiechen, M.; Kurz, P. *Angew. Chem., Int. Ed.* **2010**, *49*, 2233.
- (37) Jiao, F.; Frei, H. *Chem. Commun.* **2010**, *46*, 2920.
- (38) Yagi, M.; Narita, K. *J. Am. Chem. Soc.* **2004**, *126*, 8084.
- (39) Narita, K.; Kuwabara, T.; Sone, K.; Shimizu, K.; Yagi, M. *J. Phys. Chem. B* **2006**, *110*, 23107.
- (40) Brimblecombe, R.; Swiegers, G. F.; Dismukes, G. C.; Spiccia, L. *Angew. Chem., Int. Ed.* **2008**, *47*, 7335.
- (41) Limburg, J.; Vrettos, J. S.; Liable-Sands, L. M.; Rheingold, A. L.; Crabtree, R. H.; Brudvig, G. W. *Science* **1999**, *283*, 1524.
- (42) Naruta, Y.; Sasayama, M.; Sasaki, T. *Angew. Chem., Int. Ed. Engl.* **1994**, *33*, 1839.
- (43) Gao, Y.; Akermark, T.; Liu, J.; Sun, L.; Akermark, B. *J. Am. Chem. Soc.* **2009**, *131*, 8726.
- (44) Morita, M.; Iwakura, C.; Tamura, H. *Electrochim. Acta* **1977**, *22*, 325.
- (45) Morita, M.; Iwakura, C.; Tamura, H. *Electrochim. Acta* **1977**, *23*, 331.
- (46) Gorlin, Y.; Jaramillo, T. F. *J. Am. Chem. Soc.* **2010**, *132*, 13612.
- (47) Morita, M.; Iwakura, C.; Tamura, H. *Electrochim. Acta* **1979**, *24*, 357.
- (48) El-Deab, M. S.; Awad, M. I.; Mohammad, A. M.; Osaka, T. *Electrochem. Commun.* **2007**, *9*, 2082.
- (49) Mohammad, A. M.; Awad, M. I.; El-Deab, M. S.; Okajima, T.; Ohsaka, T. *Electrochim. Acta* **2008**, *53*, 4351.
- (50) Trasatti, S. *Electrochim. Acta* **1984**, *29*, 1503.
- (51) Singh, R. N.; Singh, J. P.; Cong, H. N.; Chartier, P. *Int. J. Hydrogen Energy* **2006**, *31*, 1372.
- (52) Fujimura, K.; Izumiya, K.; Kawashima, A.; Akiyama, E.; Habazaki, H.; Kumagai, N.; Hashimoto, K. *J. Appl. Electrochem.* **1999**, *29*, 765.
- (53) Izumiya, K.; Akiyama, E.; Habazaki, H.; Kumagai, N.; Kawashima, A.; Hashimoto, K. *Electrochim. Acta* **1998**, *43*, 3303.
- (54) Perez-Benito, J. F.; Brillas, E.; Pouplana, R. *Inorg. Chem.* **1989**, *28*, 390.
- (55) Imanishi, A.; Okamura, T.; Nakamura, R.; Nakato, Y. *J. Am. Chem. Soc.* **2007**, *129*, 11569.
- (56) Giovanol, R.; Stahli, E.; Feitknecht, W. *Helv. Chim. Acta* **1970**, *53*, 209.
- (57) Burns, R. G.; Burns, V. M. *Philos. Trans. R. Soc. London, Ser. A* **1977**, *286*, 283.
- (58) Ching, S.; Landrigan, J. A.; Jorgensen, M. L. *Chem. Mater.* **1995**, *7*, 1604.
- (59) Kanoh, H.; Tang, W.; Makita, Y.; Ooi, K. *Langmuir* **1997**, *13*, 6845.
- (60) Wu, M.; Guo, Z.; Jow, J. *J. Phys. Chem. C* **2010**, *114*, 21861.
- (61) Kwon, K. D.; Refson, K.; Sposito, G. *Geochim. Cosmochim. Acta* **2009**, *73*, 4142.
- (62) Sherman, D. M. *Geochim. Cosmochim. Acta* **2005**, *69*, 3249.
- (63) In the pH range from 9 to 12, the spectral shape and position of the intermediate species were essentially the same before and after the first rise of the current density, indicating the generation of essentially the same species as a precursor for water oxidation.
- (64) Wilson, R. H. *J. Electrochem. Soc.* **1980**, *127*, 228.
- (65) Salvador, P.; Gutierrez, C. *J. Phys. Chem.* **1984**, *88*, 3696.
- (66) Bard, A. J.; Faulkner, L. R. *Electrochemical Methods: Fundamentals and Applications*, 2nd ed.; Wiley: New York, 2001; p 590.
- (67) Davies, G. *Coord. Chem. Rev.* **1969**, *4*, 199.
- (68) Bard, A. J.; Parson, R.; Jordan, J. *Standard Potentials in Aqueous Solution*; CRC Press: New York, 1985; p 429.
- (69) Klewicki, J. K.; Morgan, J. J. *Geochim. Cosmochim. Acta* **1999**, *63*, 3017.
- (70) Klewicki, J. K.; Morgan, J. J. *Environ. Sci. Technol.* **1998**, *32*, 2916.
- (71) Webb, S. M.; Bargar, J. R.; Dick, F. J.; Tebo, B. M. *Proc. Natl. Acad. Sci. U.S.A.* **2005**, *102*, 5558.
- (72) Ronson, T. K.; McQuillan, A. J. *Langmuir* **2002**, *18*, 5019.
- (73) Nakamura, R.; Nakato, Y. *J. Am. Chem. Soc.* **2004**, *126*, 1290.
- (74) Tonkin, J. W.; Balistrieri, L. S.; Murray, J. W. *Appl. Geochem.* **2004**, *19*, 29.
- (75) Lume-Pereira, C.; Baral, S.; Henglein, A.; Janata, E. *J. Phys. Chem.* **1985**, *89*, 5772.
- (76) Baral, S.; Lume-Pereira, C.; Janata, E.; Henglein, A. *J. Phys. Chem.* **1985**, *89*, 5779.
- (77) Baral, S.; Lume-Pereira, C.; Janata, E.; Henglein, A. *J. Phys. Chem.* **1986**, *90*, 6025.
- (78) Silvester, E.; Manceau, A.; Drits, V. A. *Am. Mineral.* **1997**, *82*, 962.
- (79) Drits, V. A.; Silvester, E.; Gorshkov, A. I.; Manceau, A. *Am. Mineral.* **1997**, *82*, 946.
- (80) Sakai, N.; Ebina, Y.; Takada, K.; Sasaki, T. *J. Phys. Chem. B* **2005**, *109*, 9651.
- (81) Bard, A. J.; Faulkner, L. R. *Electrochemical Methods: Fundamentals and Applications*, 2nd ed.; Wiley: New York, 2001; p 112.
- (82) Wang, Y.; Stone, A. T. *Geochim. Cosmochim. Acta* **2006**, *70*, 4463.